The structure of full-length AFPK supports the ACP linker in a role that regulates iterative polyketide and fatty acid assembly

Heidi L Schubert[1*], Feng Li[2*], Christopher P. Hill[1], Eric W. Schmidt[2]

[1]Department of Biochemistry; [2]Department of Medicinal Chemistry, University of Utah, Salt Lake City, UT 84112.
*Authors HLS and FL are considered co-first authors.
Correspondence: CPH, chris@biochem.utah.edu; EWS, ews1@utah.edu

ABSTRACT

The polyketide synthases (PKSs) in microbes and the cytoplasmic fatty acid synthases in humans (FASs) are related enzymes that have been well studied. As a result, there is a paradigm explaining in general terms how FASs repeatedly use a set of enzymatic domains to produce simple fats, while PKSs use the domains in a much more complex manner to produce pharmaceuticals and other elaborate molecules. However, most animals also have PKSs that do not conform to the rules described in microbes, including a large family of enzymes that bridge fatty acid and polyketide metabolism, the animal FAS-like PKSs (AFPKs). Here, we present the cryoelectron microscopy structures of two AFPKs from sea slugs. While the AFPK resemble mammalian FASs, their chemical products mimic those of PKSs in complexity. How then does the architecture of AFPKs facilitate this structural complexity? Unexpectedly, chemical complexity is controlled not solely by the enzymatic domains, but is aided by the dynamics of the acyl carrier protein (ACP), a shuttle that moves intermediates between these domains. We observed interactions between enzyme domains and the linker-ACP domain, which when manipulated, altered the kinetic properties of the enzyme to create new compounds. This unveils elaborate mechanisms and enzyme motions underlying lipid and polyketide biochemistry across the domains of life.

SIGNIFICANCE

Polyketides and lipids are important in biology and medicine. Almost all of the structural and biochemical work on polyketide biosynthetic machinery describes microbial systems. Animals nearly always have their own unique sets of polyketide synthases, including newly described families that are not found in microbes, and for which almost nothing is known. One class of these enzymes is more closely related to mammalian fatty acid biosynthesis and yet makes elaborate polyketides. We describe unique enzyme states that have not been previously observed in other systems. These results highlight the unexplored biosynthetic potential of animals and the divergence of their lipid making systems in nature.

INTRODUCTION

Fatty acids and the more complex polyketides comprise major lipids, biological signalling molecules, clinically relevant therapeutics, and many other types of compounds (1–3). Polyketide synthases (PKSs) and the related cytoplasmic fatty acid synthases (FASs) in animals are mega-

enzymes that synthesize these small molecules starting from acyl-CoA derivatives (1, 4–8). The enzyme structures have three major regions: condensing, modifying, and acyl carrier protein (ACP). The enzyme's condensing region selects substrates and condenses them together through the action of acyltransferase (AT) and ketosynthase (KS) domains, respectively. The modifying region often contains ketoreductase (KR), dehydrogenase (DH), methyltransferase (MT), and enoylreductase (ER) domains that modify intermediates. Modifying domains may be active or residual (structural, ^{0}), and some may be used or skipped during a particular step in the synthetic cycle leading to diverse oxidation patterns along the polyketide chains (4, 6, 9). Finally, an ACP acts as a shuttle, carrying substrates and the growing intermediates between catalytic active sites. ACP is activated by the addition of 4'-phosphopantetheine (pPant), the carrier for substrate thioesters. The ACP-pPant makes several independent protein-enzyme interactions, which contribute to processivity and avidity (10–13). Iterative PKSs (iPKSs) and the human cytoplasmic FAS use a single set of enzymatic domains repeatedly to process all substrates and intermediates until the final product is synthesized (1, 7, 14).

Despite substantial advances, fundamental questions remain about the structure and function of animal FAS (aFAS) and iPKSs. As a result, it is currently challenging to predict the elaborate polyketides produced by iPKSs, or to engineer desired functions into FAS or iPKS enzymes. The aFAS-like PKSs (AFPKs) are intermediate in character between the human FAS and the traditionally studied type I iPKSs and provide new insights into both aFAS and iPKS function (15–17). More than 6,300 AFPKs have been identified, forming a clade with aFAS. Unlike FASs that synthesize fully reduced fatty acids, the AFPKs synthesize chemically diverse molecules, similar to the products of PKSs. However, thus far only EcPKS1 and EcPKS2 from the sea slug *Elysia chlorotica* have been biochemically characterized (15, 16), synthesizing compounds that may help the animals to perform photosynthesis using stolen chloroplasts (18, 19). FAS enzymes primarily use malonyl-CoA (MC) as substrates and fully reduce each extended unit into a fatty acid. In contrast, EcPKS1 and EcPKS2 accept primarily methylmalonyl-CoA (MMC) and select the use of specific modifying domains to introduce different oxidation states in a regioselective manner. EcPKS2 is inhibited by MC, while EcPKS1 is not. Unlike FAS, EcPKSs have a nonfunctional ER domain, resulting in polyenes. EcPKS1 and EcPKS2 also have key differences, producing compounds with different chain lengths and using the KR domain differently, leading to ketones at different positions on the final products (Fig. 1 and SI Appendix, Fig. S1).

We hoped to understand the biochemical and structural basis of these differences, which we expected would shed light on the function not only of AFPKs but of related FAS and PKS enzymes as well. Here, we report the full-length structure determination of EcPKS1 and EcPKS2 by single particle cryoelectron microscopy (CryoEM). The EcPKS2 structure resembles that of mammalian FAS (mFAS) (20), but also led to three main new findings. First, we describe intact, native ligands in several different states of the catalytic cycle, including MC in the AT active site, acetate and malonate in the KS, and NADPH bound in the KR. Second, we observed the pPant-ACP docked to the DH and KS domains, permitting the ACP-enzyme interfaces to be accurately mapped over the

catalytic cycle, revealing specific residues that interact with each enzyme domain and informing future engineering efforts. Third, remarkably, capture of the ACP at the KS is accompanied by an ordered ACP linker as an N-terminal extension of ACP helix α1 resulting in an asymmetric connection between the condensing and modifying regions. Mutation of residues within the modifying region that make contacts with the linker disrupts the catalytic cycle, changing substrate selectivity and inhibition, as well as oxidation patterns in the products. The ACP linker was also observed in the interaction with the DH domain. Collectively, these observations and experiments revealed how dynamic motions of the mega-synthase impact product structure.

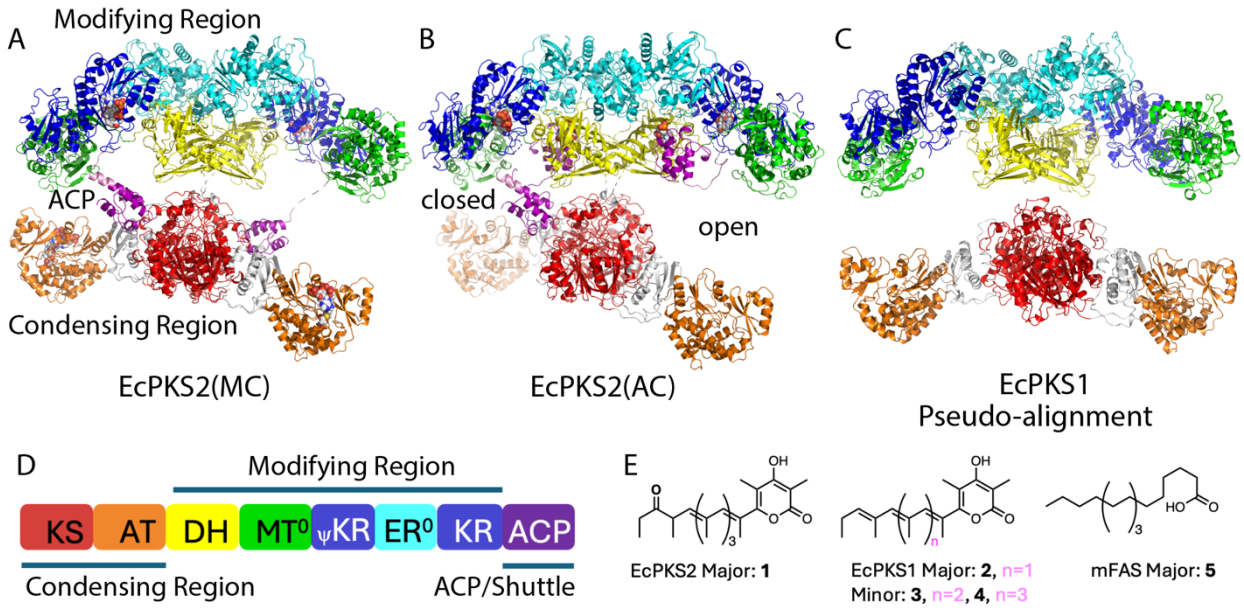

Fig. 1. Homodimeric structures and overall schematic of EcPKS1 and EcPKS2. Colors in all structures correspond with schematic in panel D. **A)** Structure of full-length EcPKS2(MC). Malonyl-CoA (MC), holo-ACP, and NADPH bound at the AT, KS, and KR active sites, respectively. Active site Cys-*S*-malonyl is present in the KS. **B)** Structure of full length EcPKS2(AC). Acylated-Cys187 at the KS domain, ACP-Acetyl-pPant docked at the DH domains and low occupancy ACP at the KS domain. **C)** EcPKS1 condensing (bottom) and modifying (top) regions in a pseudo-alignment based on EcPKS2(MC). **D)** Schematic of enzymatic domains. **E)** Primary products of EcPKS1, EcPKS2 and mFAS. Abbreviations: phosphopantetheine (pPant), ketosynthase (KS), acyltransferase (AT), dehydratase (DH), inactive methyltransferase (MT^0), ketoreductase structural domain (ψKR), inactive enoylreductase (ER^0), ketoreductase catalytic domain (KR), acyl carrier protein (ACP), mammalian FAS (mFAS).

RESULTS

EcPKS2 structure determination captures several ACP-bound states

EcPKS1 and EcPKS2 adopt the canonical "X-shaped" homodimeric structure found in mFAS (20), consistent with the close evolutionary relationship between AFPKs and mFAS enzymes (Fig. 1) (15-17, 20, 21). The RMSD between the condensing and modifying regions of EcPKS2 and mFAS

are 2.4 Å and 1.6 Å over 11,238/14,527 and 9,426/11,181 atoms respectively. The N-terminal condensing region (KS-AT didomain) tightly dimerizes through a KS:KS' domain interface, whereas the C-terminal modifying region dimerizes through the DH:DH', ER^0:$ER^{0'}$ and DH:$ER^{0'}$ domain interfaces. Large differences exist within the modification region between the AFPK/FAS structures and the PKS structures based on the inclusion or absence of entire enzymatic domains, as highlighed in work by McCullough et al (21). Models and data statistics are in SI Appendix, Table S1.

The EcPKS2(MC) full-length structure in the presence of 1 mM NADPH and MC was obtained at 3.2 Å resolution (PDB accession: 9CTL; Fig. 1A, SI Appendix Fig. S2 and S5C), revealing MC bound in the AT domain, malonate on the KS active site Cys, and NADPH bound at the KR active site. The C-terminal ACP-pPant was docked at the KS' domain active site. The linker region connecting the modifying region to this ACP forms an N-terminal helical extension of ACPα1 creating an asymmetric homodimer. The linker residues between the modifying domain and helix α1 of the ACP are fully visible in this map (SI Appendix Fig. S6F). An additional low occupancy ACP is observed in full-length reconstructions at the second KS active site with disordered linker. Contingent on the inherent symmetry of larger enzymatic regions, further focused, masked and symmetrical C2 refinement of individual condensing and modifying regions improved the resolution to 3.0 Å and 2.9 Å, respectively (PDB accession: 9CTI and 9CTK; SI Appendix Fig. S2 and S5D).

EcPKS2(AC) was determined to final resolutions of 2.9 Å and 3.1 Å for the condensing and modifying regions respectively after asymmetrical C1 refinement (PDB accession: 9CTM and 9CTN; Fig 1B, SI Appendix Fig. S3 and S5E,F). Full-length maps (2.9 Å; PDB accession: 9CTO) revealed a similar asymmetric dimer with ACP density visible at both the KS' (pPant not visible) and DH (acetyl-pPant visible) active sites, each at partial occupancy, on the closed side of the dimer. ACP'-pPant is only docked at the DH' domain at full occupancy and higher local resolution in the open side of the homodimer. While revealed with density of different strengths, the two DH-docked ACP domain interactions are modeled identically, and the EcPKS2(AC)-KS-docked ACP is modeled like that of the full-occupancy KS-docked ACP in the EcPKS2(MC) structure. Density connected to KS(Cys187) and the pPant sulfhydryl was most consistent with an acetyl group, which likely copurified from the recombinant yeast source.

EcPKS1 condensing (4.3 Å; PDB accession: 9CQ1) and modifying (3.5 Å; PDB accession: 9CQ9) were solved and refined independently (Fig 1C, SI Appendix Fig. S4 and S5B). Because of their lower resolution, EcPKS1 structures are only used in comparison with EcPKS2, and otherwise our description refers to the EcPKS2 structures.

1. Condensing region

Inhibitory malonyl-CoA adjacent to the activating nucleophile in the AT domain

The AT domain serves as the acceptance site for substrates entering the iPKS cycle and is thus central to understanding how EcPKS1 and EcPKS2 prefer methylmalonate rather than the malonate used by aFAS and fungal PKSs. Sequence analyses and experiments of bacterial AT domains have shown that residues surrounding the active site serine are predictive of substrate selectivity (22). However, alignment of iPKS, AFPK, and FAS AT sequences from fungi, bacteria, and animals reveals that these rules are not predictive in animal PKSs and AFPKs (Fig. 2C) (16, 17, 23, 24). Here, using inhibitors to stall the enzyme, we sought stuctures that would inform sequence motifs that might be more predictive in animals.

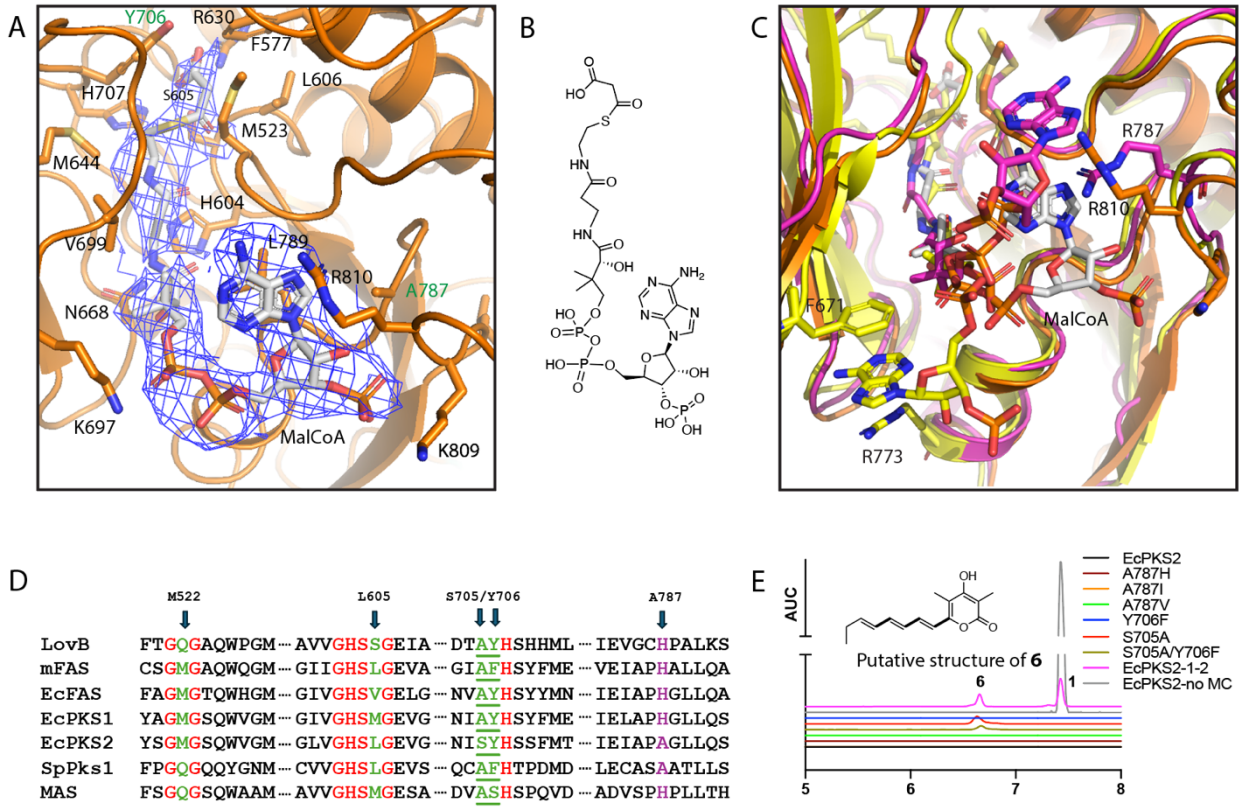

Fig. 2. Malonyl-CoA (MC) in the acyltransferase (AT) active site of EcPKS2(MC). A) MC (white) bound to the EcPKS2 AT (orange). Active site Ser605 is adjacent to the MC thioester. Residues from panel D are highlighted in their corresponding colors. **B)** Structure of MC drawn in similar orientation as shown in panel A. **C)** Comparison of CoA 3'-phosphoadenosine positions in EcPKS2(MC) (orange/white), murine FAS (PDB accession: 6ROP, yellow) (25) and murine FAS (PDB accession: 5MY0, magenta) (26), showing different orientations in all three structures. **D)** Sequence alignment of representative AT sequence motifs thought to have substrate predictive properties in bacterial PKSs (16, 17, 23, 24). Colors coordinate with panel A. Green residues 705 and 706 were mutated in panel E, while the purple residue tested MC position. **E)** Inhibition of EcPKS2 wild type and mutants after 40 min incubation with MC, MMC, and NADPH. The graph shows UPLC-MS extracted ion chromatograms (filtered for *m/z* 383.2228 and 245.1183), with the relative area under the curve shown in the y-axis and retention time on the x-axis. In gray, without MC the enzyme produces abundant **1** (product is diluted to 1/50). Production of **1** is completely suppressed by MC in wild type and all AT mutants except for the domain-swapped enzyme EcPKS2-1-2, in which a small amount of **1** is still produced. In

some of the mutants, a small amount of product incorporating three units of MC and 3 units of MMC was produced. A possible structure of the resulting compound **6** is shown; [U-^{13}C]-malonate was used to confirm the incorporation of MC (*m/z* 251.1384, SI Appendix Fig. S9B).

Despite the common use of MC as a substrate for FAS, remarkably, EcPKS2 is inhibited by MC. When glycerol from the enzyme preparation was included in the buffer, inhibition remained competitive but reversible. EcPKS2 was rapidly inactivated, with a $t_{1/2}$ of 1.4 min in the presence of 250 µM MC, with a 10 µM IC_{50} (SI Appendix Fig. S7A). Inhibition was competitive with MMC, consistent with the observation of MC in the AT active site in the structure. We used this knowledge to stall EcPKS2 in a ligand-bound state as had been shown to work for yeast FAS (27).

Addition of MC (1 mM) to the protein prior to EM grid preparation resulted in EcPKS2(MC), with MC non-covalently bound to the EcPKS2 AT domain at a local resolution of ~3.5 Å (Fig. 2A and SI Appendix Fig. S6A). The MC carboxylate moiety interacts with the ring face of active site Tyr706 and experiences charge offset through proximity to His707 and Arg630. Catalytic Ser605 is positioned 3.4 Å from the target carbonyl. The position of the MC in the active site suggests that it should be a substrate of the AT, and not an inhibitor.

The large AT active site pocket facilitates only weak interactions (distances between 3.9-4.9 Å) with the cysteamine and β-alanine regions of the CoA, including polar interactions with Asn668, Thr674 and Met523. Hydrophobic residues Val699, Leu789 and Leu790 surround the dimethyl carbons of the pantoic acid region, and Lys697 interacts with the first bridge phosphate (Fig. 2A and 2B). In a FAS:octanoyl-CoA complex, the nucleotide is packed against the ferredoxin-like domain between residues Phe671 and Arg773, and in the CoA-bound FAS, where MC has already been transferred to the active site Ser, the nucleotide is at the interface between AT-subdomains packing against conserved Arg787 which plays a dual role in nucleotide positioning and formation of a salt bridge with the bridging phosphate (25, 26). MC in EcPKS2(MC) most closely resembles the CoA-bound mFAS where the 3'-phosphoadenosine group is positioned on the outer surface of the active site pocket interacting with loop residues Ala787-Gly788-Leu789, and again an arginine (Arg801) near the nucleotide. Critically, the Ala787-Gly788 pair permits close association of the nucleotide with the AT domain unique to other CoA-bound structures. To test whether the phosphoadenosine position affects MC binding or inhibition, mutations of EcPKS2 Ala787 to His, Val and Ile were constructed and assayed, but remained inhibited (Fig. 2E). These residues were selected because they were observed in other AFPKs, including those that might be associated with MC use as a substrate.

Most of the residues previously shown in bacterial PKS to impact substrate selectivity (22, 23, 28) are uninformative in EcPKS1 and EcPKS2 due to sequence divergence. Based upon the structure of EcPKS2, the homologous residues are adjacent to the bound MC (Fig. 2A), yet sequence alignments and mutational experiments show that they are not diagnostic of substrate selectivity. For example, residues M523 and L606 are at selectivity-determining positions in bacteria (22),

but they are not diagnostic in EcPKS1 and 2, which have M/L in position 606 yet both select MMC (Fig. 2D). Residues Ser705-Tyr706 corresponded to the VASH motif in the bacterial iPKS, mycoseric acid synthase (MAS), which natively uses MMC. When the MAS Ser was mutated to Phe, the mutant protein preferentially accepted MC instead of MMC (28, 29). Based upon this precedent, EcPKS2 was mutated to Ala705, Phe706, or Ala705-Phe706, which were anticipated to be more substrate permissive. These EcPKS2 mutants were still inhibited by MC (Fig. 2E). There was a small but noticeable increase in the incorporation of MC into products, which using mass spectrometry of labeled and unlabeled intermediates were most consistent with structure **6** (Fig. 2). However, in contrast to **1** which can be isolated and was previously characterized by NMR (16)**,** the amount synthesized was minute, so that it could not be well characterized. Mutations outside of the AT led to a more pronounced (but still minor) **6** production (Fig. 2D, and see below). Thus, the best studied residues affecting PKS substrate selectivity did not alter EcPKS2 products, implicating alternative mechanisms of substrate selection.

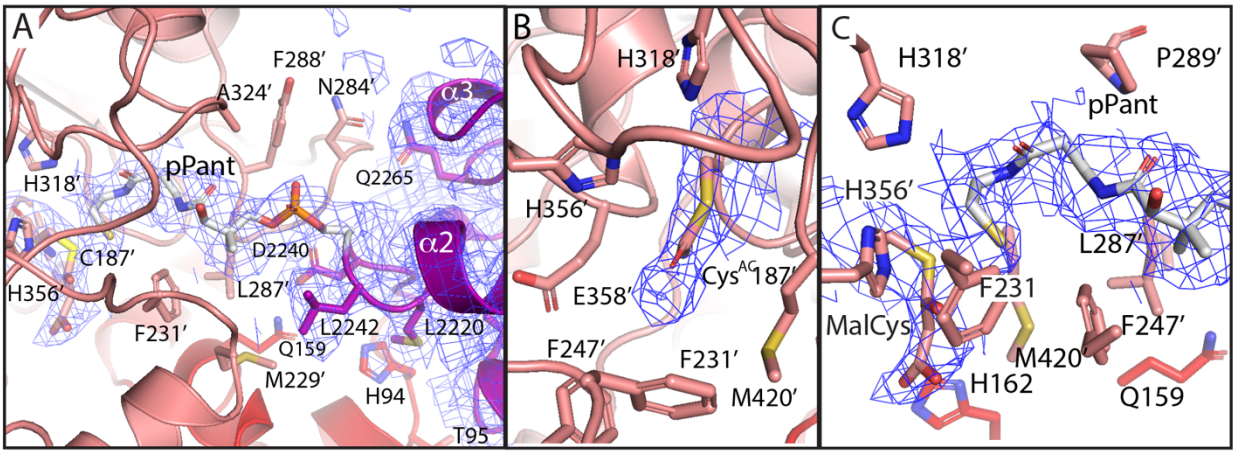

Fig. 3. EcPKS2 ketosynthase (KS) active sites. A) EcPKS2(MC) KS with ACP-pPant bound. Residues surrounding the pPant (white) and at the interface between the KS (red), KS' (pale red) and ACP (purple). **B)** Residues surrounding the EcPKS2(AC) KS active site acetylated-Cys187'. **C)** Density for Cys-loaded malonate (MalCys) is found in EcPKS2(MC). The ACP-bound pPant also converges on the active site.

Active states of KS with ACP-pPant and covalently bound Cys *S*-malonyl or Cys *S*-acetyl

KS domains catalyze the condensation of the elongating acyl chain with an extender unit, comprised of MMC in the case of EcPKS2. The EcPKS2 KS was previously shown to be involved in controlling the chain length (16). The KS domain active sites are opposed at the central dimer interface of the condensing region (Fig. 1). In EcPKS2(MC), ACP is bound at this KS:KS' interface making interactions through the end of ACP(α1), the beginning of ACP(α2), and the middle of ACP(α3). These interactions span the KS:KS' interface such that ACP(Asp2240:OD1) interacts with KS Gln159:OE1, ACP(Met2243:SC) interacts with KS His94, and ACP(Leu2220:O) interacts with KS Thr95, but ACP(Gln2265 and Leu2242) interact with Asn284' and Met229' of the subunit housing the active site residues and a pocket (Fig. 3A). The KS catalytic residues, EcPKS2(His318', His356'

and Cys187'), are within the opposing polypeptide chain from the ACP. The position of the ACP is similar to that previously reported for Lsd14 (7S7C) and GfsA (8IN9), and an overlay is presented in SI Appendix Fig. S8C.

The EcPKS2(MC) covalently bound pPant extends from Ser2241 into the KS pocket towards the Cys187' active site residue (Fig. 3A). The sulfhydryl group of pPant was modeled near the active site of Cys187' but was not covalently bound (SI Appendix Fig. 6B). Like the malonyl-CoA bound in the AT, no direct hydrogen bonds are formed with the pPant, although a hydrophobic ring comprising EcPKS2 residues Phe231, Tyr288 and Ala324 stabilizes the pantoic acid dimethyl group. Additional density extends from the Cys187' sulfhydryl, suggestive of a covalently bound malonyl group from MC. This is normally the position in which a starter unit awaits the pPant-linked extender unit. This suggests that the inhibition of EcPKS2 by MC might be at least in part mediated by the KS. Similarly, other groups have previously suggested that the KS domain regulates the transacylation step in aFAS (30).

Along these same lines, the EcPKS2(AC) reconstruction displays density most consistent with the presence of a covalently linked acetyl group on the catalytic cysteine residue (Fig. 3B and SI Appendix Fig. S6C). The acetyl may be residual from yeast acetyl-CoA ligands. Only discontinuous density is present within the pPant tunnel. Nonetheless, in EcPKS(AC), a low occupancy ACP is visible outside the KS active site in similar position to that seen in the EcPKS(MC) structure (Fig. 5B,D and SI Appendix Fig. S5E). These states mimic what might happen when a substrate-loaded ACP binds, transfers its substrate to the active-site Cys residue, then leaves the active site.

2. Modifying region

Inactive domains

The inactive MT^0 and ER^0 domains are ordered and adopt canonical enzyme conformations but lack active site residues and are not used by the enzymes (20, 31) (Supporting information).

KR domain is observed with NADPH bound

The β-KR domain catalyzes the reaction after Claisen condensation to reduce a β-ketoester to a β-hydroxyester through oxidation of NADPH. Density for NADPH is visible in the EcPKS2 KR active site of both structures, but the flexible substrate-binding loop (2154-2158) is disordered (SI Appendix Fig. S6D). EcPKS2(AC) active site residues Tyr2117, Lys2076 and Ser2104 are near the nicotinamide riboside, positioned similarly to what is observed in the structure of human FAS bound to NADPH and a spiro-imidazolone inhibitor (16, 24, 32). In EcPKS2(MC) the NADPH structure sits a bit higher, and the density is much worse for the nicotinamide mononucleotide and substrate-binding loop, emphasizing the differences in conformational flexibility of this

region that result from rigidification upon substrate-triggered loop closure that pushes NADP further into the pocket.

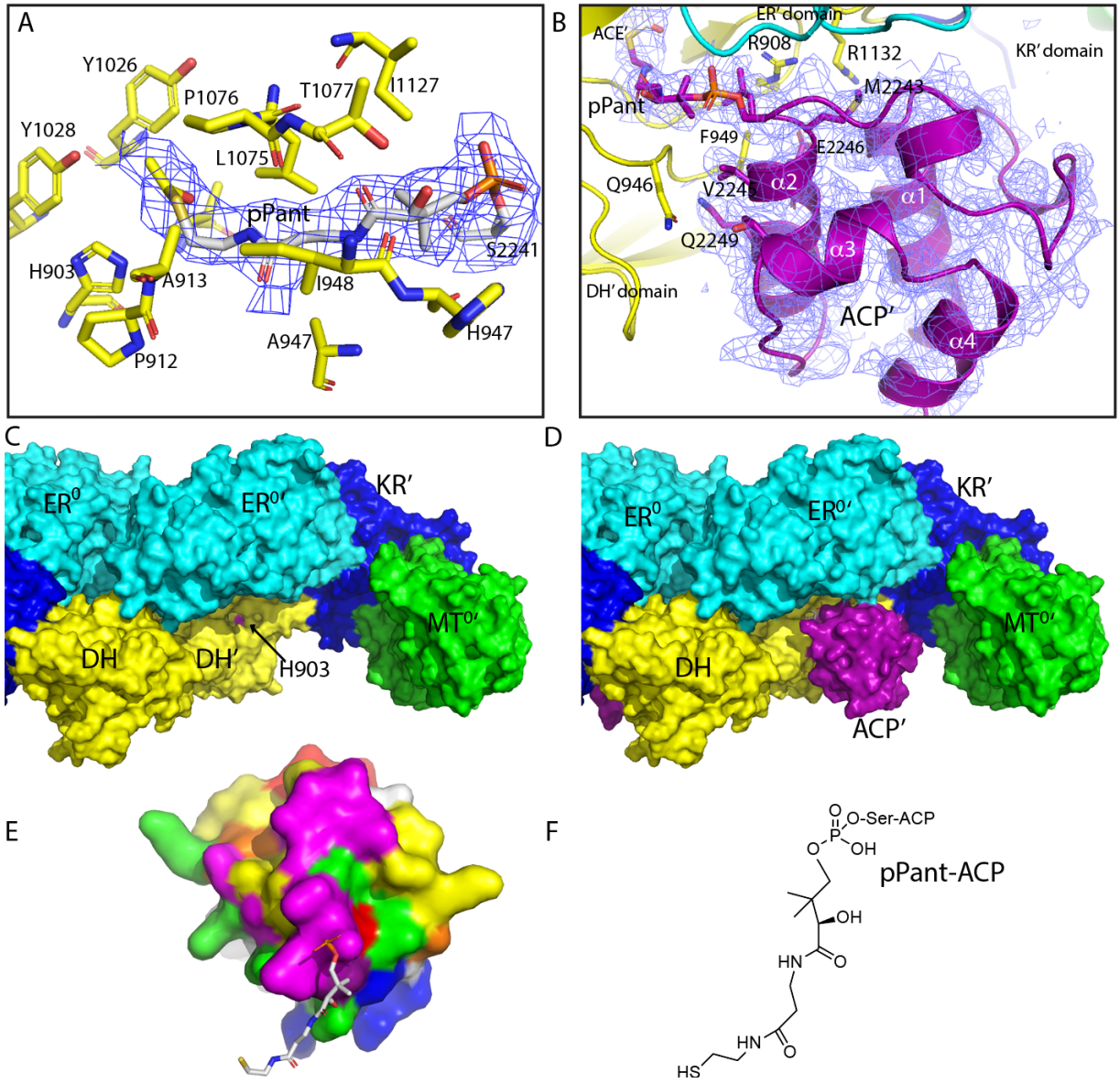

Fig. 4. ACP-acetylated-pPant docked at the dehydratase (DH) domain in EcPKS2(AC). A) DH (yellow) active site surrounding the acetylated-pPant (white). **B)** ACP' (purple) interface with DH' (yellow) domain with nearby surfaces of ER$^{0'}$ (cyan) and KR' (blue) domains. **C)** Molecular surface of EcPKS2 modifying region colored by enzymatic domain. The substrate tunnel in the apo-DH (yellow) domain (pink His903). **D)** Surface shown in C with the ACP' (magenta) docked at the DH (yellow) domain. **E)** Surface of the ACP domain with residues colored by the respective interactions with the AT, KS and DH domains. ACP interactions marked with DH (blue), KS (red) and AT (orange) interactions as well as those residues which overlap at the DH:AT (green), KS:AT (yellow) and DH:KS (deep purple) or all three interfaces (magenta). **F)** Chemical structure of ACP-bound pPant in a similar orientation as in E.

DH domain and its interface with ACP

DH domains eliminate the hydroxyl group created by the KR, generating a double bond. The EcPKS2 DH comprises a pseudo internal repeat of α+β "hot dog" folds. In the EcPKS2(AC) structure, ACP lies below the ER domain pointing the Ser2241:pPant into DH active site, the first time this has been observed for a FAS-like DH domain (Fig. 4 and 5). Additional density for the pPant is visible past the sulfhydryl group, which lies between the active site residues His903 and Asp1058. An acetyl group has been modeled off of the sulfhydryl, consistent with the density found at the KS active site in this structure (Fig. 4A and SI Appendix Fig. S6E). The pPant pocket is lined with hydrophobic residues including Val905, Ile944, Ala947, Tyr1026, Leu1075, Thr1077, and Ile1127, with the carbonyl oxygens of Ile944 and His945 just beyond (3.5-4Å) hydrogen-bonding distance of the hydroxyl of the pantothenic acid moiety. Mutation of His903 to Ala resulted in abortive products (SI Appendix Fig. S10B) (16), indicating that the mutations abolished DH domain activity. The ACP':DH' interface comprises the surface of ACP(α2) and includes hydrogen bonds from Gln2249'(NE2) to Gln946'(OE1) and Ala947'(O) and GLN2249'(OE1) to Phe949'(N) as well as van der Waals interactions surrounding the phenyl ring of DH':Phe949' with ACP' residues Leu2242', Val2245', Gln2246' and Gln2249' (Fig. 4B).

3. ACP

ACP-enzyme domain interface specificity

We observed the ACP docked to both the KS and DH domains within full-length AFPK structures, and its conformation can be predicted at the AT domain by homology to other known structures (Fig. 3, 4, and S8) (33, 34). The three domains make some distinct interactions with a few different residues of ACP but generally overlap in their interaction with the pPant and its nearby region. Charge and hydrophobic surface complementarity dominate the interactions, along with a few hydrogen bonds. The DH:ACP interface has a slightly smaller solvent inaccessible interface of 527 $Å^2$ while the KS:KS':ACP interface is 675 $Å^2$ (SI Appendix Fig. S8). Mapping residues on the ACP that lie at various enzyme interfaces (Fig. 4E) reveals ACP residues specific to binding individual enzyme domains. Given the variable residues found in these ACP positions (SI Appendix Fig. S11), it is likely that the evolution of this interface will have to be taken into account in designing engineered FAS and PKS enzymes.

A structured ACP linker impacting mega-enzyme motion

The ACP domain is increasingly regarded as crucial to substrate processivity. In the FAS/AFPK families, the linker between the KR and ACP domain comprises 8-17 small hydrophilic residues that are thought to be flexible and enable freedom of motion of the ACP. Truncations of this linker and cross-linking have been used as tools to restrict ACP movement and catch ACP docked at active sites (10, 35, 36). Many modular PKSs contain additional domains that are C-terminal to

the ACP to further restrict and regulate ACP function. Previous reports have not resolved the linker residues, leaving unanswered the question of how the most flexible region of the ACP might participate in producing the diverse array of polyketide and fatty acid derived compounds.

Remarkably, in the full-length EcPKS2(MC), one ACP is rigidly tethered between the KS and MT^0 structural domain (Fig. 1A, 1B, 5A and SI Appendix Fig. S6F). The ACP linker leaves the KR domain at residue Val2195 and continues in an extended conformation towards the MT^0 domain to a turn at residue Gly2200 (Fig. 5A). The Ser2198 hydroxyl hydrogen bonds with Trp1333 within the MT^0 domain and Gly2200 packs tightly against the face of Trp1333. The final linker residues adopt a helical structure, which directly extends into the first helix of the canonical four-helix bundle of the ACP domain. A second ACP at lower occupancy is visibly docked at the opposing KS' active site, but the linker is not visible (SI Appendix Fig. S2) consistent with a mechanism whereby the order and disorder of the linker accommodates a see-saw motion of the condensing region with respect to the modifying region. The AT and KS active sites (and the KR and DH active sites) lie on opposite sides of the central x-y plane (as defined in Fig. 1A-C) and motion of the condensing region is necessary for passage of the ACP from the KS to the AT, and likewise from the KR to the DH (Fig. 6).

We wondered whether the linker orientation could be observed for the ACP docked at the DH domain. If so, they might indicate other defined linker interactions important in catalysis. A 6 Å low-pass filter map for the EcPKS2(AC) structure revealed density visible at low contour for the linker in multiple conformations. Linkers were visible at high occupancy between the KR' and the DH'-docked ACP'. The linker extends away from KR' and joins the start of ACP': α1 at residue 2207 (Fig. 5C). On the other side of the homodimer, the linker conformation for ACP docking at KS' in EcPKS2(AC) is similar to what was seen in EcPKS2(MC), but now overlaps with the partial occupancy linker to the second DH domain (Fig. 5D). The EcPKS2(AC) structure highlights the contortions required by the linker to convert from an ordered helical extension to an extended coil. Note that the ACP docked at the KS could not simply swivel down to the DH but would require motions of condensing and modifying regions to provide additional space for that trajectory (Fig. 6).

Previous work has documented a wide range of motion between the condensing and modifying domains of mFAS (12). Conformational heterogeneity between the condensing and modifying regions is so great in the EcPKS1 dataset that the full-length structure could not be reconstructed, and analysis by CryoSPARC 3DFlex failed to provide meaningful insight. In the EcPKS2 datasets the full-length structures are constrained by the docked ACP to the KS and ordered linker. Heterogeneity was investigated using CryoSPARC 3DFlex analysis of EcPKS2(MC), revealing an x-axis wobble of the condensing domain with respect to the modifying domain (Supplemental Movie), but no evidence is present for significant y- or z-axis rotations (where axes are defined in the orientation of Fig. 1A-C). Motion is observed radiating out from the fulcrum caused by the ACP-linker tether.

Structured ACP linker modulates catalytic activity

These observations suggested that the ability of the linker to form an ordered structure may help keep the rotational flexibility in check for enzyme efficiency and substrate progression. We therefore proposed that the greater chemical complexity of EcPKS2 products might result from a stronger linker interaction than is present in either EcPKS1 or FAS. For example, among other possibilities perhaps the ketone in **1** is present because the affinity for the linker leads to a slightly longer dwell time of the ACP in the KS active site. Speculatively, a structured linker-enzyme interaction in EcPKS2 might slightly stabilize the KS-docked state. In turn, if the first reduction at the KR is slightly kinetically disfavored, a longer dwell time at the KS might favor the formation of double bond during first cycle. It should be emphasized here that there are many other possibilities, but that they converge on a role that the linker in enzyme dynamics and mobility impacts the products of the mega-synthase.

To test this hypothesis, two different strategies were used. In the first, we aimed to convert the EcPKS2 linker interface to be more EcPKS1-like sequence, and vice versa. In the second, we compared EcPKS2 linker-ACP to residues present in aFAS enzymes.

Three key EcPKS2 residues responsible for forming the ordered linker conformation, Ser2198 from the linker and Trp1333/Gln1334 from MT^0, were identified and compared with corresponding residues in EcFAS and EcPKS1 (Fig. 5E). This region was not found in the phylogenetically distant bacterial PKS, but it could be observed throughout the aFAS and AFPKs (SI Appendix Fig. S11 and S12), as well as in more distantly related fungal PKS (Fig. 5E). While residues were variable within this alignment, linker alignment followed a pattern in which FAS formed its own clade with similar residues, while those in the AFPKs were more variable.

On the basis of these comparisons, we mutated the corresponding residues in EcPKS1 to produce single mutant EcPKS2(Ser2198Val) and triple mutant EcPKS2-SWQ/VYR. The single mutant had no observable effect on the enzyme and will not be further discussed. The converse triple mutant, EcPKS1-VYR/SWQ, was also expressed and purified. To compare EcPKS2 with EcFAS, glutamates 2004 and 2205 were mutated to Gly, to produce EcPKS2-EE/GG. In contrast to the SWQ interface residues, the EE residues in EcPKS2 are found at the base of the helix, just after the linker. The hydrophilic EcPKS2 EE linker residues support the extended helix into the ACP that the EcFAS GG residues are not expected to mimic. The double and triple mutants impacted the enzyme in three ways. First, the product spectrum in the presence of MMC and NADPH was affected by mutations. In assays with wild-type EcPKS2, the vast majority of product was ketone-containing **1**. Only <4% of products lacked ketone and instead were reduced to the olefins **3** and **4**. With EcPKS2-SWQ/YVR, the ratio was modestly increased, but with EcPKS2-EE/GG a full 10% of products were reduced, representing a >2.5-fold increase in use of the KR:DH domains (Fig. 5F, SI Appendix Fig. S7).

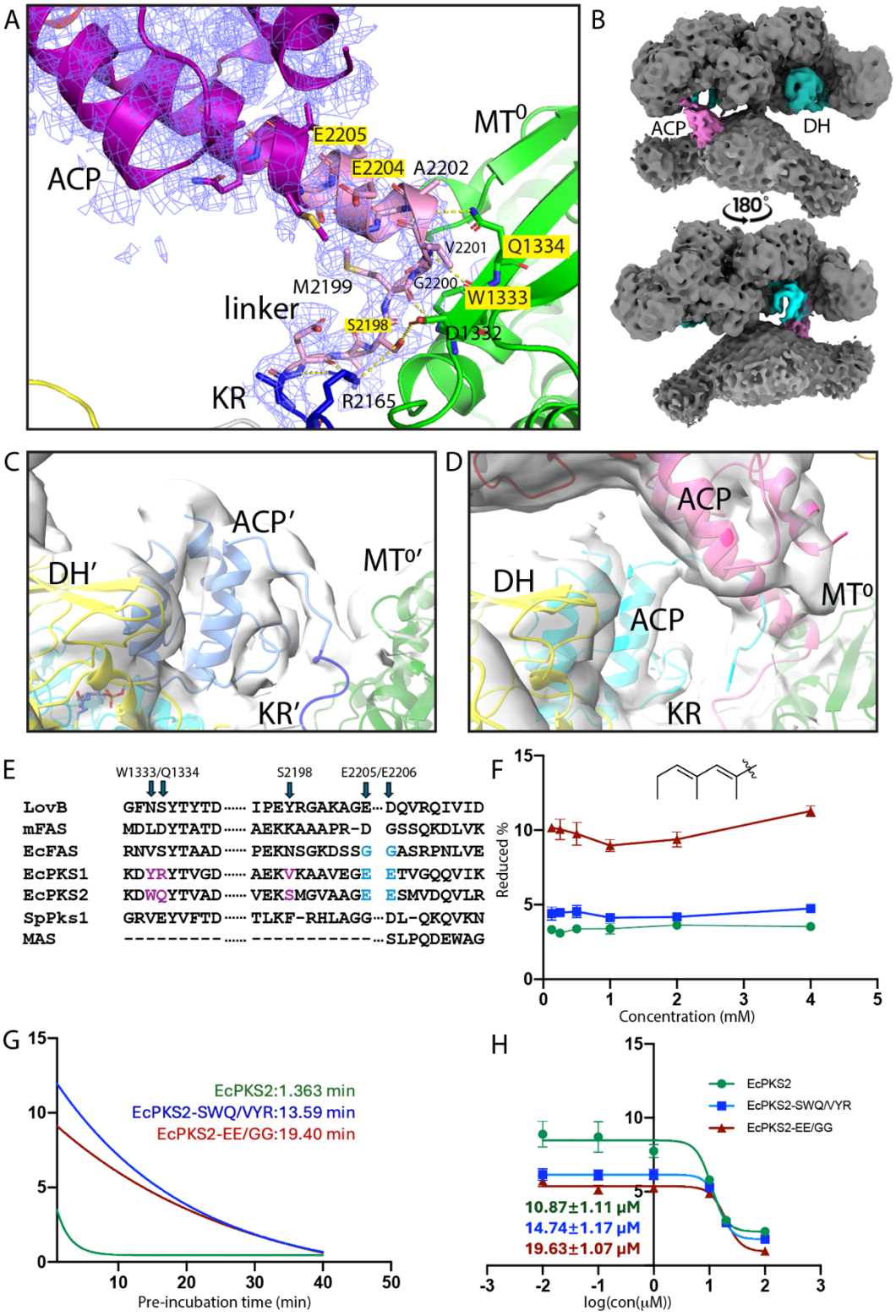

Fig. 5. Structure of the ACP linker. A) Interactions between the EcPKS2(MC) ACP linker and KR and MT^0 domains. MT^0 domain (green), KR domain (blue), ACP linker (pink) and ACP domain (purple). Reisdues selected for mutation are highlighted in yellow. **B)** Low contour maps of full-length EcPKS2(AC) revealing three bound ACPs. The open side

of the homodimer reveals the ACP partially occupied at both the KS (pink) and DH (cyan) domain while the other side of the homodimer only contains the DH-docked ACP (darker cyan). Two panels are flipped 180 degrees on the y-axis to reveal back of protein. **C)** 6 Å low-pass filter of the map shown in panel B at low contour shows the linker between the KR' domain and ACP' docked at the DH' domain in EcPKS2(AC). **D)** Map in C viewed at the DH, KR, MT^0 region revealing partial occupancy ACPs at both the DH and the KS domains with alternative linkers visible to both. **E)** ACP linker (EcPKS2, residues 2198-2206) and converse MT^0 face (EcPKS2 1330-1339) sequence alignment using FAS, iPKS, and AFPK sequences (numbering based upon EcPKS2). These identify linker mutants used in panels F, G and H. **F)** An increase in the percent of reduced products is observed when the ACP linker is mutated. In the y-axis, reduced % was calculated as the ratio of reduced products (**3** and **4**) over the total products, with the concentrations representing AUC measurements made by UPLC-MS. In the x-axis, MMC concentration is shown **G)** Malonyl-CoA (MC) inhibition ($t_{1/2}$) of linker mutants with 250 mM MC. The y-axis is area under the curve (AUC) of compounds **1** and **1**' (structure shown in SI Appendix Fig. S7). **H)** MC inhibition of linker mutants. The inset values show the MC IC_{50} in µM for each mutant. The x-axis shows the log[MC] (µM), while the y-axis shows AUC of compounds **1** and **1**'. Statistics are provided for panels D-F in SI Appendix Fig. S13.

A second difference was observed in response to the presence of MC. All three EcPKS2 double and triple mutants were inhibited, but the mutants were inhibited to a lesser degree and incorporated MC as a starter unit, making compound **1'** in addition to **1**. Inhibition by MC was measured, showing that EcPKS2, EcPKS2-SWQ/YVR, and EcPKS2-EE/GG had IC_{50}s of 10, 15, and 20 µM, and $t_{1/2}$s at 250 mM of 1.4, 14, and 19.4 min, respectively (Fig. 5G and H).

The third major difference was in the overall enzyme kinetics in the presence of MMC and NADPH. Wild type EcPKS1 is not inhibited by MC, and slower than EcPKS2. Making the EcPKS2 linker more EcPKS1-like slowed the enzyme down, while the converse experiment increased the rate of EcPKS1. The EcPKS2-SWQ/YVR k_{cat}/K_m and V_{max} were decreased by ~25% in comparison to wild type (SI Appendix Fig. S7B). Conversely, EcPKS1-VYR/SWQ had double the k_{cat}/K_m in comparison to wild type enzyme (SI Appendix Fig. S7B2,C). EcPKS1 is a slow enzyme, and the increase in its rate with this simple change is significant. Moreover, it is much harder to improve native enzyme function than to break it; a significant increase in rate with such a minor change in a putatively "unstructured" region of an enzyme, well outside of any functional regions or enzyme domains, is noteworthy. Collectively, these results suggest that the ACP is much more than a carrier of intermediates. When we increased the flexibility of the linker in EcPKS2, we observed an increase in the activity of the KR for the first reduction and a decrease in inhibition by MC, accompanied by a decrease in the catalytic efficiency of the enzyme. This suggests that a change in mobility alters the kinetics of interactions between the enzymatic domains and the substrate-linked ACP.

Application of ACP linker to enzyme engineering

Finally, we aimed to determine whether insights into the linker region could be used to improve enzyme engineering. In previous work, we hybridized the EcPKS1 condensing region with the modifying region and ACP from EcPKS2, and vice versa, aiming to make new products. For

example, the enzyme with EcPKS2 condensing region and EcPKS1 modifying/ACP regions was named "EcPKS2-1". The resulting enzymology strongly implicated the KR as dictating the reduction pattern, and the KS as dictating the chain length (16), since products **3** and **4** lacked the ketone, consistent with the EcPKS1 modifying region, but were longer in chain length, consistent with the EcPKS2 condensing region.

We hypothesized that using the EcPKS2 linker in a hybrid context with the EcPKS1 KR might restore the ketone. Therefore, we created a new hybrid, EcPKS2-1-2, in which the modifying domain of EcPKS1 was joined to the condensing domain of EcPKS2; the ACP and its linker, at Val2194, were joined to the C-terminus of the EcPKS1 modifying domain (Table S4). When MMC and NADPH were incubated with purified EcPKS2-1-2, we obtained both the reduced product expected from the EcPKS1 KR, but also the ketone-containing product (SI Appendix Fig. S9). This supports the hypothesis that the linker-ACP is important in controlling product regioselectivity. In addition, when MC was added with MMC and NADPH, we saw an increase in malonate-derived products **6** and **2'** (Fig. 2E, SI Appendix Fig. S9B, **2'** structure in SI Appendix Fig. S7C). This last observation implies that global changes to the enzyme kinetics modify either AT substrate loading or the acceptance of malonate-containing extended products in the mega-synthase.

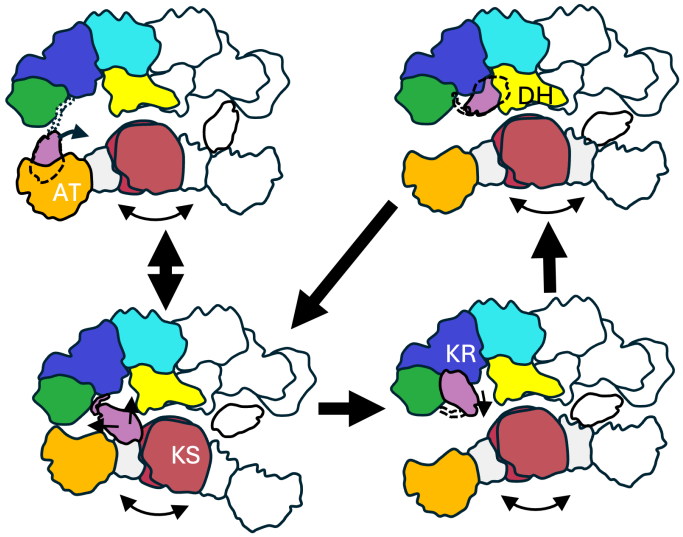

Fig. 6. Schematic of domain and ACP movement expected during one side of the mega-enzyme active site cycle. Arrows below the condensing domains reflect necessary motions to allow the ACP to access the front and back sides of the dimer. Dotted lines reflect the flexibility or structure of the ACP-linker and the presence of the ACP at a front-side active site (solid lines) or backside active site (dotted lines).

Discussion

The thousands of AFPKs found in animal genomes bridge an evolutionary gap between FAS and PKS enzymes (15), which is reflected in the close structural relationship between EcPKS2 and the

previously described mFAS (20, 37, 38). However, AFPKs make complex polyketides such as **1** instead of FAS product **5**. Some of the polyketide-like features of **1** and related compounds are readily explained based upon the structure and sequence of EcPKS2 in comparison to microbial precedents. For example, the structure of ER^0 (Fig. 1) shows mutations that disrupt the catalytic active site while retaining the structural domain, similar to what is found in fungal iPKSs such as LovB from lovastatin biosynthesis, explaining why the double bond cannot be reduced and instead **1** is a polyene (30, 36). Pyrones are often products of fungal iPKS enzymes when the offloading domian is absent or disrupted (36). The C-terminus of EcPKS2 is an ACP, rather than the thioesterase that terminates FAS and offloads the free acid, explaining the presence of pyrone.

The reasons underlying other differences between AFPK and FAS products, such as regioselective reduction by the KR (SI Appendix Fig. S1) and substrate selectivity, were more challenging to elucidate. AFPKs are closely related to both fungal iPKSs and aFASs, yet the latter two primarily use MC (8). Initially, we hoped that enzyme structures would reveal an obvious reason for this difference. Because MC inhibited EcPKS2, we added it to the enzyme preparation, providing the first structure including this important native ligand. Although EcPKS2(MC) is probably useful in understanding AT function, neither the structure itself, nor the obvious mutations, provided significant insights into MMC usage. The differences between EcPKS1 and EcPKS2 will be invaluable as a model in future studies for testing the molecular mechanisms and kinetics of individual domains, and how those impact FAS and PKS products.

Instead, what emerged from this study was the central role of enzyme motions and ACP interactions in directing product synthesis. We observed the interaction of the ACP in several native enzyme states, revealing co-evolution of residues specific for the interface between ACP and individual enzyme domains like recent studies in yeast (39,40). ACP-bound states also unveiled unanticipated interactions between the ACP-linker and the mega-synthase. The linker connecting the ACP to the rest of the enzyme is not always flexible and disordered, as previously believed, but has the potential to make specific contacts with enzyme domains. It was remarkable that two point mutations altering a flexible region of the mega-synthase resulted in a significant shift in the resulting chemistry, especially in the KR regioselectivity.

The presence of these multiple structures enabled us to construct an accurate model for the motions that occur over the course of the catalytic cycle (Fig. 6). In the EcPKS2(AC) structure, an acetyl-CoA from the recombinant yeast system entered the catalytic cycle as a starter unit, but was unable to function as an extender unit, trapping EcPKS2(AC) in a “start-unit-cycled” state, directly effecting the location of the docked ACP domains. The structure displays asymmetry, with the compressed side exhibiting a mixture of KS- and DH-docked ACP and the open side displaying primarily a DH-docked ACP. This suggests that the distance between the condensing and modifying regions effects the equilibrium of the ACP at the various active sites. The presence of acetyl in the KS domain prevents significant association of the acetyl-pPant-ACP with the KS;

instead, the enzyme is stalled one step earlier at the end of the modifying cycle, within the DH domain. By contrast, EcPKS2(MC) is locked in an MC-inhibited state with ACP in a KS-docked pose.

The difference between these states requires a specific set of enzyme motions. As the ACPs carry intermediates between active sites within the homodimer, the modifying and condensing regions must see-saw back and forth (z-axis) to allow the ACP to pass (Fig. 6). Additional rotational motions along the y-axis may facilitate access of ACP to both faces of each region (in front and behind the image plane drawn in Fig. 1. The structure exemplifies the dynamic and dependent nature of the opposing sides of the homodimer, in which space is needed to cross between active sites that lie on either side of the x-y plane. It is unlikely that the ACP tethered to the KS domain could detach and reach the nearby AT domain without concomitant z-axis rotation of the two regions. Rotational dynamics would permit ACP access from one face of the homodimer (backside of Fig. 1 for KR and AT active sites) to the other (front side of Fig. 1 for DH and KS active sites). During the rotational acrobatics, the linker region would be expected to fold and unfold to permit access to the four active sites, but additional rotational limitations may be imposed due to torsion restraints. These dynamics could in part explain why changes in overall enzyme kinetics via the ACP-linker interaction would lead to differences in active site access, and hence the final chemistry of the enzyme.

Our results impact broader understanding of FAS and PKS biochemistry in several ways. Overall, the structures we report have substantial similarity to mFAS, but add key features not previously observed. First, our work provides what we believe is the first example of a DH-docked ACP structure, which based upon sequence homology is presumably similar in the FAS enzymes. Second, while Brignole et al. (12) found conformational heterogeneity between mFAS condensing and modifying regions, a detailed analysis was not possible due to a lack of stalled intermediates. Here, we now show how an AFPK with close structural similarity to FAS undergoes conformational changes. Third, in previous work the impact of the linker between ACP and TE in aFAS was mapped, allowing chain length alteration through modification of the linker (41). Here, we investigated the linker connecting all other enzymatic domains to the ACP and demonstrate in structural detail factors responsible for enzymatic products, which can inform engineering to modify activities such as regioselectivity, among others. While PKSs are more distantly related, they have some key features that are informed by our study. For example, the fungal iPKSs are the closest relatives of the aFAS/AFPK clade, and also perform regioselective reactions. The stalling of MC and malonate/acetate in the EcPKS KS and AT active sites closely reflect aspects of starter- and extender-unit selectivity in those homologous enzymes that have not been observed. Thus, our structural analysis can help guide understanding of related enzymes.

More fundamentally, aFAS shares a common ancestor with the AFPKs, both of which arose from fungal iPKS or similar enzymes (17). Different types of FAS have also emerged across the kingdom of life, including the individual domains of the type II FAS in bacteria, plastids, and mitochondria, the expanded octameric yeast FAS found in fungi and some bacteria, and the homodimeric aFAS

(8). In these cases, there are closely related PKSs that perform reactions with more complex regiochemistry. Our results suggest that the ACP and ACP-linker interactions and dynamics provide a straightforward evolutionary route between complex regiochemical outcomes found in PKSs and the simpler ones found in FAS, perhaps helping to explain the convergent solutions to fatty acid and polyketide biosynthesis that have emerged across the tree of life.

Methods

Detailed methods are provided in the Supporting Appendix. Mollusc proteins EcPKS1 and EcPKS2 and their mutants synthesized in this study were expressed and purified as previously described (15,16). Proteins in 0.08% Tween-20 were immobilized on grids and data collected on either on a Titan KRIOS or a KRIOS 4. EcPKS2(MC) was created by first adding 1 mM NADPH and MC, while EcPKS2(AC) used benzoyl-CoA and NADPH. Purified enzymes were used for enzyme assays with substrates MMC, MC, NADPH, and other acyl CoAs. Time-course, yield, and kinetic experiments were performed by monitoring reaction conditions in at least two biological replicates, each with triplicate technical replicates, with significance determined using a t-test.

Supplemental Movie

3D-flexibility observed within the EcPKS2(MC) dataset. Two latent coordinate series showing motions radiating out from the ACP-linker fulcrum are depicted here. One (in yellow) reveals more y-axis motion compressing and releasing the distant AT domain versus the distant KR/MT while the second (in blue) reveals more x-axis motion rolling the condensing region side to side with respect to the modifying region.

Data Availability

Primary CryoEM micrographs and model coordinates were deposited at the EMDB and PDB databases (SI Appendix, Table S1).

Acknowledgement. This work was funded by NSF 2203613. We would like to acknowledge use of the University of Utah Electron Microscopy core facility. The support and resources from the Center for High Performance Computing at the University of Utah are gratefully acknowledged. A portion of this research was supported by NIH grant R24GM154185 and performed at the Pacific Northwest Center for Cryo-EM (PNCC) with assistance from Marzia Miletto at OHSU and accessed through EMSL (grid.436923.9), a DOE Office of Science User Facility sponsored by the Office of Biological and Environmental Research. The authors wish to thank Zhenjian Lin (U. Utah) for sequence analysis support.

References

1. C. Hertweck, The biosynthetic logic of polyketide diversity. *Angew. Chem. Int. Ed.* **48**, 4688–4716 (2009).

2. J. Staunton, K. J. Weissman, Polyketide biosynthesis: a millennium review. *Nat. Prod. Rep.* **18**, 380–416 (2001).
3. S. Smith, S.-C. Tsai, The type I fatty acid and polyketide synthases: a tale of two megasynthases. *Nat. Prod. Rep.* **24**, 1041–1072 (2007).
4. A. T. Keatinge-clay, The uncommon enzymology of *cis*-acyltransferase assembly lines. *Chem. Rev.* **117**, 5334–5366 (2017).
5. C. S. Heil, S. S. Wehrheim, K. S. Paithankar, M. Grininger, Fatty acid biosynthesis: chain-length regulation and control. *ChemBioChem* **20**, 2298–2321 (2019).
6. J. Wang, Z. Deng, J. Liang, Z. Wang, Structural enzymology of iterative type I polyketide synthases: various routes to catalytic programming. *Nat. Prod. Rep.* **40**, 1498–1520 (2023).
7. M. Grininger, Enzymology of assembly line synthesis by modular polyketide synthases. *Nat. Chem. Biol.* **19**, 401–415 (2023).
8. D. A. Herbst, C. A. Townsend, T. Maier, The architectures of iterative type I PKS and FAS. *Nat. Prod. Rep.* **35**, 1046–1069 (2018).
9. T. Robbins, Y.-C. Liu, D. E. Cane, C. Khosla, Structure and mechanism of assembly line polyketide synthases. *Curr. Opin. Struct. Biol.* **41**, 10–18 (2016).
10. L. Buyachuihan, F. Stegemann, M. Grininger, How Acyl Carrier Proteins (ACPs) Direct Fatty Acid and Polyketide Biosynthesis. *Angew. Chem. Int. Ed.* **202312476** (2023).
11. J. Crosby, M. P. Crump, The structural role of the carrier protein--active controller or passive carrier. *Nat. Prod. Rep.* **29**, 1111–1137 (2012).
12. E. J. Brignole, S. Smith, F. J. Asturias, Conformational flexibility of metazoan fatty acid synthase enables catalysis. *Nat. Struct. Mol. Biol.* **16**, 190–197 (2009).
13. J. T. Mindrebo, *et al.*, "Structural Basis of Acyl-Carrier Protein Interactions in Fatty Acid and Polyketide Biosynthesis" in H.-W. (Ben) Liu, T. P. B. T.-C. N. P. I. I. I. Begley, Eds. (Elsevier, 2020), pp. 61–122.
14. A. M. Soohoo, D. P. Cogan, K. L. Brodsky, C. Khosla, Structure and mechanisms of assembly-line polyketide synthases. *Annu. Rev. Biochem.* **93**, 471–498 (2024).
15. J. P. Torres, Z. Lin, J. M. Winter, P. J. Krug, E. W. Schmidt, Animal biosynthesis of complex polyketides in a photosynthetic partnership. *Nat. Commun.* **11**, 2882 (2020).
16. F. Li, *et al.*, Animal FAS–like polyketide synthases produce diverse polypropionates. *Proc. Natl. Acad. Sci.* **120**, e2305575120 (2023).
17. Z. Lin, F. Li, P. Krug, E. Schmidt, The polyketide to fatty acid transition in the evolution of animal lipid metabolism. *Nat. Commun.* **15**, 1–13 (2024).
18. M. E. Rumpho, E. J. Summer, J. R. Manhart, Solar-powered sea slugs. Mollusc/algal chloroplast symbiosis. *Plant Physiol.* **123**, 29–38 (2000).
19. B. J. Green, *et al.*, Mollusc-algal chloroplast endosymbiosis. Photosynthesis, thylakoid protein maintenance, and chloroplast gene expression continue for many months in the absence of the algal nucleus. *Plant Physiol.* **124**, 331–342 (2000).
20. T. Maier, M. Leibundgut, N. Ban, The crystal structure of a mammalian fatty acid synthase. *Science* **321**, 1315–1322 (2008).

21. T. M. McCullough, *et al.*, Structure of a modular polyketide synthase reducing region. *Structure* **31**, 1109–1120 (2023).
22. S. F. Haydock, *et al.*, Divergent sequence motifs correlated with the substrate specificity of (methyl) malonyl-CoA : acyl carrier protein transacylase domains in modular polyketide synthases. *FEBS Lett.* **374**, 246–248 (1995).
23. F. Li, *et al.*, Sea urchin polyketide synthase SpPks1 produces the naphthalene precursor to echinoderm pigments. *J. Am. Chem. Soc.* **144**, 9363–9371 (2022).
24. S. M. Ma, Y. Tang, Biochemical characterization of the minimal polyketide synthase domains in the lovastatin nonaketide synthase LovB. *FEBS J.* **274**, 2854–2864 (2007).
25. A. Rittner, K. S. Paithankar, A. Himmler, M. Grininger, Type I fatty acid synthase trapped in the octanoyl-bound state. *Protein Sci.* **29**, 589–605 (2020).
26. A. Rittner, K. S. Paithankar, K. V. Huu, M. Grininger, Characterization of the polyspecific transferase of murine Type i fatty acid synthase (FAS) and implications for polyketide synthase (PKS) engineering. *ACS Chem. Biol.* **13**, 723–732 (2018).
27. K. Singh, *et al.*, Reconstruction of a fatty acid synthesis cycle from acyl carrier protein and cofactor structural snapshots. *Cell* **186**, 5054-5067.e16 (2023).
28. B. J. Dunn, C. Khosla, Engineering the acyltransferase substrate specificity of assembly line polyketide synthases. *J. R. Soc. Interface* **10** (2013).
29. S. Dutta, *et al.*, Structure of a modular polyketide synthase. *Nature* **510**, 512–517 (2014).
30. A. Witkowski, A. K. Joshi, S. Smith, Mechanism of the β-ketoacyl synthase reaction catalyzed by the animal fatty acid synthase. *Biochemistry* **41**, 10877–10887 (2002).
31. J. Wang, *et al.*, Structural basis for the biosynthesis of lovastatin. *Nat. Commun.* **12**, 867 (2021).
32. T. Lu, *et al*., Design and synthesis of a series of bioavailable fatty acid synthase (FASN) KR domain inhibitors for cancer therapy. *Bioorg. Med. Chem. Lett.* 28(12), 2159-2164 (2018).
33. A. Miyanaga, S. Iwasawa, Y. Shinohara, F. Kudo, T. Eguchi, Structure-based analysis of the molecular interactions between acyltransferase and acyl carrier protein in vicenistatin biosynthesis. *Proc. Natl. Acad. Sci.* **113**, 1802–1807 (2016).
34. S. R. Bagde, I. I. Mathews, J. C. Fromme, C. Y. Kim, Modular polyketide synthase contains two reaction chambers that operate asynchronously. *Science (80-.).* **374**, 723–729 (2021).
35. S. Bonhomme, C. Contreras-Martel, A. Dessen, P. Macheboeuf, Architecture of a PKS-NRPS hybrid megaenzyme involved in the biosynthesis of the genotoxin colibactin. *Structure* **31**, 700-712.e4 (2023).
36. M. Dell, *et al.*, Trapping of a polyketide synthase module after C-C bond formation reveals transient acyl carrier domain interactions. *Angew. Chem. Int. Ed.* **202315850** (2023).
37. D. A. Herbst, R. P. Jakob, F. Zähringer, T. Maier, Mycocerosic acid synthase exemplifies the architecture of reducing polyketide synthases. *Nature* **531**, 533–537 (2016).
38. Q. Zhang, B. Pang, W. Ding, W. Liu, Aromatic polyketides produced by bacterial iterative type i polyketide synthases. *ACS Catal.* **3**, 1439–1447 (2013).

39. E. K. Samani, *et al.*, Direct structural analysis of a single acyl carrier protein domain in fatty acid synthase from the fungus *Saccharomyces cerevisiae*. *Commun. Biol.* **7**, 92 (2024).
40. K. Singh, G. Bunzel, B. Graf, K.M. Yip, M. Neumann-Schaal, H. Stark, A. Chari, Reconstruction of a fatty acid synthesis cycle from acyl carrier protein and cofactor structural snapshots. Cell 186(23), 5054-5067.e16 (2023).
41. A. K. Joshi, A. Witkowski, H. A. Berman, L. Zhang, S. Smith, Effect of modification of the length and flexibility of the Acyl Carrier Protein− Thioesterase interdomain linker on functionality of the animal fatty acid synthase. *Biochemistry* **44**, 4100–4107 (2005).